



Research paper

Hybrid path planning method for USV using bidirectional A* and improved DWA considering the manoeuvrability and COLREGs

Donghao Xu ^{a,b}, Jie Yang ^a, Xueqian Zhou ^{b,d}, Haitong Xu ^{c,d,*}^a College of Automation, Harbin University of Science and Technology, Harbin, 150080, China^b College of Shipbuilding Engineering, Harbin Engineering University, Harbin, 150001, China^c Centre for Marine Technology and Ocean Engineering (CENTEC), Instituto Superior Técnico, Universidade de Lisboa, Lisbon, Portugal^d International Joint Laboratory of Naval Architecture and Offshore Technology Between Harbin Engineering University, University of Lisbon, Harbin, 150001, China

ARTICLE INFO

Keywords:

Bidirectional A* algorithm
 Dynamic window algorithm
 Unmanned surface vessel
 COLREGs
 Manoeuvrability

ABSTRACT

This paper proposes a hybrid dynamic path planning algorithm that integrates global path planning (GPP) and local path planning (LPP). The objective is to effectively address the challenges associated with path planning and collision avoidance for unmanned surface vehicles (USV) in complex environments. The bidirectional A* algorithm is used to search the optimized strategy based on the actual geographical information map for the navigation routes of USV. The Dynamic Window Algorithm (DWA) is employed, and a novel cost function is formulated considering the USV's manoeuvring characteristics, dynamic constraints, and environmental information. The primary purpose is to ensure the compliance of the USV with COLREGs during dynamic obstacle avoidance. It accomplishes this by providing positive reinforcement for achieving the correct turning speed when the USV determines the orientation of an approaching ship. Another evaluation function is introduced to mitigate the problem of local optima in complex environments that the LPP may encounter. The actual work map is used to model the application scenario with the obstacles in the presence of incoming ships, the simulation results show that the proposed algorithm is capable of generating adaptive, collision-free routes while adhering to COLREGs rules.

1. Introduction

Unmanned Surface Vehicles (USVs) represent an autonomous navigation platform within the realm of marine robotics. (Er et al., 2023; Fernando et al., 2023). USVs have a wide range of applications in both military and civilian fields (Hosseini et al., 2018; Liu and Guedes Soares, 2023, 2024), including environmental monitoring (Zhang et al., 2020), maritime surveillance (Yang et al., 2023; Ye et al., 2024; Yuan et al., 2022), depth measurement (Chen et al., 2023), and special operations support (Cai and Li, 2022). To ensure the safety of USVs during operations, path planning aims to facilitate the secure and efficient navigation of USVs to their destination within complex environments. Improved path planning contributes to achieving this objective by enabling USVs to reach their destination at a more optimal speed, minimizing energy consumption, and enhancing overall operational efficiency (Xing et al., 2023; Xu et al., 2023). Additionally, the integration of autonomous collision avoidance technology is a key element in the development of the planning path.

The concept of path planning finds its roots in the field of mobile robotics. Fox et al. (1997) pioneered a methodology wherein a robot adeptly chooses a trajectory with assured dynamic constraints. This approach enables the robot to optimize its translational speed, minimize the angle to the target, and uphold a secure distance from obstacles. Khatib (1986) introduced an innovative robotic manipulator employing the "artificial potential field" concept for instantaneous obstacle avoidance in mobile robots. Kuffner and LaValle (2000) proposed a path planning algorithm for high-dimensional configuration spaces based on rapidly exploring random trees and greedy heuristic search algorithms. Applying path planning algorithms to USVs confronts numerous challenges, including unmodeled uncertainty (Fossen, 2011), environmental disturbance (such as wind, wave, and water current) (Wang et al., 2022), and navigation rules (Sun et al., 2023). Overlooking these factors in path planning not only leads to significant energy wastage during the operation of USVs but also increases the potential risk of collisions with other vessels in marine environments.

In recent years, numerous studies have been carried out on the path

* Corresponding author. Centre for Marine Technology and Ocean Engineering (CENTEC), Instituto Superior Técnico, Universidade de Lisboa, Lisbon, Portugal.
 E-mail addresses: xudonghao@hrbust.edu.cn (D. Xu), haitong.xu@centec.tecnico.ulisboa.pt (H. Xu).

planning of USVs. The challenges associated with path planning are categorized into global path planning problems, reliant on a priori environmental data, and local path planning problems, contingent upon sensor information. Global path planning (GPP) is mainly achieved through point-to-point search methods, including the Dijkstra algorithm (Sun et al., 2021), fast marching square (FMS) method (Hinostroza et al., 2018, 2019, 2021), A* algorithm (Liang et al., 2021; Shi et al., 2019; Song et al., 2019), rapidly extending random tree (RRT) algorithm (Dustin J and Berg, 2013; Gammell et al., 2014; Mao et al., 2023), D* lite method (Zhu et al., 2021) and AIS data (Xu et al., 2019; Xu and Guedes Soares, 2016). Local path planning (LPP) is usually achieved based on trajectory prediction, including artificial potential field (APF) method (Hao et al., 2023; Xu et al., 2021), velocity obstacle (VO) method (Berg et al., 2008; Zhuang et al., 2019), dynamic window approach (DWA) (Er et al., 2021; Tang et al., 2015), just to name a few.

The grid-based path planning approach, the A* algorithm, originated with the Dijkstra algorithm. This method was subsequently advanced to the A* by incorporating a heuristic cost, as proposed by Hart et al. (1968). The introduction of this heuristic aimed to expedite the search process through the pruning of the search space. This approach was introduced into USV's path planning (Liang et al., 2021), where an improved minimum course alteration algorithm (MCA) was proposed. In another study, the A* algorithm was extended by combining motion primitive constraints-based path planning system with a local threat map based on the Apollonius circle toward USV's path planning in an uncertain sea environment (Shi et al., 2019). Tang et al. (2015), proposed an adaptive adjustable fast marching square (AAFMS) for heterogeneous USVs. Rapidly Exploring Random Trees (RRT) algorithm is another widely used method for path planning, with its principal aim being the rapid expansion of a set of tree-like trajectories. This expansion is geared towards a comprehensive exploration of a significant portion of the configuration space, facilitating the identification of feasible paths (Mao et al., 2023). However, owing to the stochastic nature of the algorithm's sampling, the resulting paths are frequently feasible but suboptimal. The RRT* algorithm, as proposed by Dustin J and Berg (2013), extends the RRT algorithm by assigning a circular range to the root node. This range filters random nodes within its confines, incurring a lower computational cost for generating optimal paths. Consequently, the planned paths contribute to enhancing the performance of the RRT algorithm in terms of path length optimization. Gammell et al. (2014), proposed the informed RRT* algorithm, which employs ultra-long pheromones to characterize the subset of states to improve the search efficiency of the algorithm. The global path planning of USVs in known environments ensures effective static obstacle avoidance. Nevertheless, several challenges persist in dynamically navigating unknown environments, including issues related to real-time performance. Sun et al. (2021), improved the traditional Dijkstra algorithm based on the storage environment by using an eight-angle search method, which reduces the number of turning points of the planned path. Additionally, the study addressed the constrained steering capability of USVs in known environments by expanding the adjacent search range and establishing a safe distance parameter for USVs within storage environments.

In the research on the collision avoidance method of the APF method. Lyu and Yin (2019) proposed a modified APF for real-time path planning of USVs, which contains a new modified repulsive potential field function and corresponding virtual force. Dynamic and fast Q-learning (DFQL) was proposed by combining Q-learning with APF, and the performance of the proposed algorithm is verified with offline and online modes for USVs in different environmental conditions (Hao et al., 2023). Xu et al. (2020) introduced a dynamic collision avoidance algorithm, named LAPF-CC, leveraging a layered artificial potential field and collision cone. This algorithm minimizes inefficient collision avoidance manoeuvres by segmenting the potential field. It assesses collision risk through the consideration of relative distance and velocity as variables. In the context of the Velocity Obstacle (VO) method, Zhuang et al.

(2019) introduced a collision avoidance algorithm tailored for high-speed USVs, proficient in dynamically adjusting both the heading and speed of the USV. This choice is pivotal as traditional algorithms such as A*, FMS, and RRT demand more computational time to guarantee the completeness of collision avoidance path searches. This is particularly notable when confronted with sudden collision avoidance requirements that necessitate swift response times. Although APF and VO methods have fast response capability, they have problems such as local optimization (Fu et al., 2019), trajectory fluctuation, and difficulty in combining multiple constraints. The DWA can combine multiple constraints such as collision avoidance rules with kinematic constraints. For the DWA, Er et al. (2021), proposed an improved DWA to enable USVs to cope with real marine environments containing dynamic obstacles. (Yan et al., 2021), applied the improved DWA with the movement ability of USVs. However, dynamic obstacle avoidance of USVs in maritime environments requires compliance with relevant safety guidelines. Such as the ignorance of provisions of international regulations for preventing collision at sea (COLREGs) (Kim et al., 2021).

In addressing the limitations of a real-time global path planning algorithm and dynamic obstacle avoidance in unknown environments, this paper proposed a hybrid path planning method using the improved bidirectional A* and DWA. To enhance safety and reliability in navigation, an evaluation function for collision avoidance, aligned with the manoeuvrability and propulsion character of USV, is developed. Additionally, constraints based on path extraction points and COLREGs are incorporated, leading to the derivation of feasible dynamic trajectories for the USV. The main contributions of this paper are given as follows:

1. A bidirectional A* and COLREGs-based DWA is proposed for the hybrid path planning for USVs by utilizing an 8-neighborhood framework to enhance the efficiency of global search.
2. Incorporating the ship's manoeuvrability and propulsion characteristics, a speed sampling space is constructed for the prediction of feasible trajectories. Furthermore, a new cost function is introduced to assess and filter plausible paths.
3. Comparative studies are carried out to validate the performance of the proposed hybrid path planning method, and the numerical study in the real environment is also conducted with dynamic and unknown obstacles.

The organization of the remaining sections of this paper is as follows: Section 2 introduces the global path planning system. Section 3 presents the local path planning system and the cost functions are defined in this section. Section 4 outlines the operational steps of the hybrid dynamic path planning algorithm. Section 5 conducts simulations to validate the feasibility of the hybrid algorithm. Finally, Section 6 provides a summary of the overall work conducted in this paper.

2. Global path planning using the bidirectional A* algorithm

2.1. Global environment mapping

The modelling of a global environment involves extracting a region for path planning from the actual map captured by the satellite camera. In order to partition the accessible area Ω_0 and inaccessible area Ω_1 within the entire map domain Ω_X , grayscale processing is required on the original colour sea map $M_o(R_{(x,y)}, G_{(x,y)}, B_{(x,y)})$ to obtain the grayscale map $M_g(g_{(x,y)})$. The grayscale map $M_g(g_{(x,y)})$ can be described as follows:

$$g_{(x,y)} = \omega_1 R_{(x,y)} + \omega_2 G_{(x,y)} + \omega_3 B_{(x,y)} \quad (1)$$

where R , G and B are the degrees of the red, green, and blue, respectively, ω is the weight of these colours defined by the weighted average method to initialize the grayscale of the map.

In order to partition Ω_0 and Ω_1 , we set the grey value of Ω_0 and Ω_1 to 255 and 0, respectively:

$$\bar{g}_{(x,y)} = \begin{cases} 0 & g_{(x,y)} < \delta \\ 255 & g_{(x,y)} \geq \delta \end{cases} \quad (2)$$

where δ is a threshold. To convert the grayscale-processed sea map into a matrix consisting of '0' and '1', we designate the numeral '0' for navigable sea regions, demarcated by white grids, while '1' indicates impassable sea areas, denoted by black grids. As shown in Fig. 1.

2.2. Global path planning algorithm

The A* algorithm is widely used for path planning due to its maturity and efficiency. The hybrid dynamic path planning algorithm adopts the A* algorithm for the global path planning of USV. Given the manoeuvrability constraints of marine ships, executing a precise 90-degree turn in maritime environments poses a notable challenge. Therefore, the 8-neighborhood A* algorithm is used, which makes the USV easily track the globally planned path. An evaluation function $f(n)$ is used to evaluate path length. The basic idea is to search the optional nodes around the current node, select the least costly node, and iteratively repeat this process until reaching the target point. The function $f(n)$ is defined as:

$$f(n) = g(n) + h(n) \quad (3)$$

where $g(n)$ is the length of the path that USV has travelled from the start point n_{start} to the current node $n_{current}$, and $h(n)$ is the heuristic value which estimates the distance from $n_{current}$ to target point n_{goal} . In this paper, the heuristic function utilizes the Euclidean distance. The global path is determined through a series of steps: first, initializing the start and end points and incorporating them into the open list; then, selecting a node, expanding it, and iteratively updating the list; and finally, commencing at the endpoint of the parent node and retracing the path back to the starting point of the parent node to establish the optimal path. The corresponding pseudo-code is described in Algorithm1.

The A* algorithm necessitates the maintenance of both open and closed lists, involving actions such as addition, deletion, and update operations for each node. As the real map undergoes rasterization for broader global environmental applications, the resulting search space undergoes expansion, consequently amplifying the operational overhead associated with these actions. This, in turn, results in an escalation of both time complexity and memory usage within the algorithm, thereby influencing the efficiency of path planning. To address this challenge, this paper adopts a bi-directional search strategy within the A* algorithm. This strategy facilitates simultaneous searches originating from both the initial and terminal points until a solution connecting the two search queues is identified. When compared to the conventional A* algorithm, this method diminishes the sizes of the open and closed lists, thereby mitigating memory consumption and computational overhead.

The corresponding pseudo-code is given in Algorithm 2.

```

Data:  $n_{start}$ ,  $n_{goal}$ , open_list, close_list
Result: path from  $n_{start}$  to  $n_{goal}$ 
1 Initialize open_list = { }
2 Initialize close_list = { }
3  $n_{start} \rightarrow$  open_list
4 while open_list ≠ { } do
5    $n_{current}$  = the node in the open_list with the smallest  $f(n)$ 
6   open_list ← open_list -  $n_{current}$ 
7   close_list ← close_list +  $n_{current}$ 
8   if  $n_{current} = n_{goal}$  then
9     | return path from  $n_{start}$  to  $n_{goal}$ 
10    end
11   foreach  $n_i \in$  eight neighborhoods of  $n_{current}$  do
12     | if  $n_i \neq$  obstacle  $\wedge n_i \notin$  open_list  $\wedge n_i \notin$  close_list then
13       | |  $n_i \rightarrow$  open_list
14       | |  $n_{current}=n_i.parents$ 
15       | | calculate  $f(n_i)$ ,  $g(n_i)$ , and  $h(n_i)$ 
16     | end
17     | if  $n_i \in$  open_list then
18       | | if  $f'(n_i) < f(n_i)$  then
19         | | |  $f(n_i) = f'(n_i)$ 
20         | | |  $n_{current}=n_i.parents$ 
21       | | end
22     | end
23   end
24 end
```

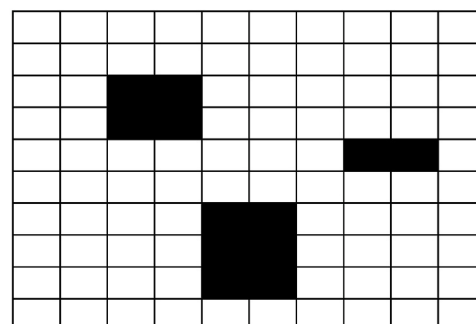
Algorithm 1. A* Algorithm.

In the context of this research, the progression from the initial point to the destination is formally labelled as a forward search, while the investigation from the destination to the starting point is referred to as a backward search. As shown in Algorithm 2, both the forward and backward search processes iteratively adjust the destination point, facilitating a prompt convergence of their respective paths. When the expanded node $n_{i,f}$ of the current node $n_{current,f}$ in the forward search encounters either the current node $n_{current,b}$ of the backward search or the expanded node $n_{i,b}$ of the current node $n_{current,b}$ in the backward search encounters the current node $n_{current,f}$ of the forward search, the termination condition for the bidirectional search process is met.

Based on the above method, the USV determines the globally optimal path from the start point to the endpoint, and the USV navigating along this path ensures avoidance of collisions with obstacles on the global map. Simultaneously, it identifies extraction points along the global path to guide the local path planning of the USV. The rules governing the extraction of these path points are outlined as follows:

0	0	0	0	0	0	0	0	0	0
0	0	0	0	0	0	0	0	0	0
0	0	1	1	0	0	0	0	0	0
0	0	1	1	0	0	0	0	0	0
0	0	0	0	0	0	0	1	1	0
0	0	0	0	0	0	0	0	0	0
0	0	0	0	1	1	0	0	0	0
0	0	0	0	1	1	0	0	0	0
0	0	0	0	1	1	0	0	0	0
0	0	0	0	0	0	0	0	0	0

(a) Two-dimensional array



(b) Grid map

Fig. 1. Two-dimensional grid map.

1. The inflection point of a globally planned path is mandated as a path extraction point.
2. Both the commencement and termination points are inherently deemed path inflection points.
3. If the linear span between two inflection points exceeds a predefined distance, supplemental extraction points are systematically introduced at equidistant intervals along the trajectory.
4. Path extraction points serve as provisional target points for local path planning.
5. Upon reaching a path extraction point, the Unmanned Surface Vehicle (USV) reaches the status of a temporary goal point, with the subsequent path extraction point taking on the role of the next target point.

3. Local path planning using improved DWA

Assuming a comprehensive understanding of both the environmental factors and obstacle data, the A* algorithm effectively plans the global path during navigation. However, unanticipated circumstances, such as unregistered obstacles like reefs and mobile obstacles like incoming ships, present collision risks to USVs within the global environment. In the absence of prompt intervention, a collision between the USV and obstacles becomes a noteworthy safety concern. To ensure safe navigation and real-time obstacle avoidance, this section advocates employing the Dynamic Window Approach (DWA) with local obstacle avoidance capabilities for fine-tuning local path planning.

3.1. Mathematical model of USV

In order to design the controller for USVs, a requisite component involves the formulation of a mathematical model. This section introduces the kinematic model of the USV. Within the realm of ship motion and path planning, the focus of research is on the variations of posture angle and navigation trajectories, particularly the horizontal plane motion of the vessel. In order to simplify the model of the USV, only the motion in the horizontal plane is considered and the following constraints are made.

- 1) The roll, pitch, and heave motions of the USV are excluded.
- 2) The dynamic equations governing the USV do not encompass disturbance forces, such as waves, wind, and ocean currents.

For USVs, the effect of vertical swing, longitudinal, and transverse rocking motion on the motion in the horizontal plane is negligible. Consequently, the motion of a USV can be accurately represented by the standard three-degrees-of-freedom vessel model encompassing surge, sway, and yaw. As shown in Fig. 2, XOY is the Earth-centered Inertial (ECI) coordinate, and xoy is the body-fixed coordinate. The angle ψ is the yaw angle of USV in XOY. In xoy, r is the angular velocity in yaw, u and v are linear velocities in surge and away. A typical USV kinematic model with unperturbed horizontal plane motion can be expressed as:

$$\dot{\eta} = J(\eta)v \quad (4)$$

where $\eta = [x \ y \ \psi]^T$ is the position vector of USV in the body-fixed coordinate system, $v = [u \ v \ r]^T$ is its velocity vector in three degrees of freedom, $J(\eta)$ is the transformation matrix between the two coordinate systems:

$$J(\eta) = \begin{bmatrix} \cos \psi & -\sin \psi & 0 \\ \sin \psi & \cos \psi & 0 \\ 0 & 0 & 1 \end{bmatrix} \quad (5)$$

Substituting Equation (5) into Equation (4), the kinematic equations of USV can be established as:

$$\begin{cases} \dot{x} = u \cos(\psi) - v \sin(\psi) \\ \dot{y} = u \sin(\psi) + v \cos(\psi) \\ \dot{\psi} = r \end{cases} \quad (6)$$

3.2. Velocity sampling space design

In order to simulate the trajectory of viable velocity pairs (u, r) , it is crucial to determine the surge speed range $[u_{\min}, u_{\max}]$ and the yaw rate range $[r_{\min}, r_{\max}]$ during simulation period before employing the LPP methodology. These ranges are subdivided into three components within the velocity sample space:

- a. Due to the inherent mechanical constraints of the USV propulsion and steering system, the maximum and minimum boundary limits exist for both its surge speed and yaw rate. The velocity space V_m that can be sampled at this point is: (kinematic constraints of propulsion and steering system)

$$V_m = \{(u, r) | u \in [u_{\min}, u_{\max}] \wedge r \in [r_{\min}, r_{\max}]\} \quad (7)$$

where u_{\max} is the maximum surge speed and r_{\max} is the maximum yaw rate, u_{\min} is the minimum surge speed and r_{\min} is the minimum yaw rate. Because the inversion of the propeller is not considered in the paper, the minimum surge speed $u_{\min} = 0$ m/s.

- b. The limited output torque of the propeller and rudder, when incorporated into the USV imposes constraints on both the acceleration of surge speed and yaw rate. As a result, the velocity space V_d , that can be sampled at this juncture is as follows: (Dynamic constraints of propulsion and steering system)

$$V_d = \{(u, r) | u \in [u_c - \dot{u}_s \Delta t, u_c + \dot{u}_a \Delta t] \wedge r \in [r_c - \dot{r}_s \Delta t, r_c + \dot{r}_a \Delta t]\} \quad (8)$$

where u_c and r_c are the surge speed and yaw rate of the USV; \dot{u}_a and \dot{u}_s are the maximum surge speed acceleration and the maximum surge speed deceleration; \dot{r}_a and \dot{r}_s are the maximum yaw rate acceleration and the maximum yaw rate deceleration; Δt is the time step.

- c. In the context of velocity determination, it is imperative to restrict the sampling space in consideration of the braking distance. In instances where the Unmanned Surface Vehicle (USV) encounters obstacles in the course of navigation, it is essential to reduce the sampled velocity to zero before the USV coming into contact with the obstacle. Consequently, within a singular simulation cycle, the sampled surge speed becomes instrumental in facilitating the USV's prompt cessation before colliding with any obstacles. This limitation on the velocity space for sampling is imposed as a safety constraint.

$$V_a = \left\{ (u, r) \mid u < \sqrt{2 \cdot dist(u, r) \cdot \dot{u}_s} \wedge r < \sqrt{2 \cdot dist(u, r) \cdot \dot{r}_s} \right\} \quad (9)$$

where $dist(u, r)$ is the closest distance between the predicted trajectory of the feasible velocity pairs (u, r) and the obstacles.

In conclusion, the final selected velocity sampling space V_s is the intersection of the three aforementioned sets. Let V_s represent the admissible velocity set, then V_s should satisfy the following:

$$V_s = V_m \cap V_d \cap V_a \quad (10)$$

As shown in Fig. 3, The black rectangular region represents the velocity sampling space V_m constrained by the kinematic constraints of the propulsion and steering system, the yellow region represents obstacles, the red region represents the velocity sampling space V_a constrained by safety constraints, the blue region represents the velocity sampling space V_d constrained by the propulsion system dynamic constraints, and the green region represents the final velocity sampling space V_s .

Data: $\text{open_list}_{\text{forward}}$, $\text{close_list}_{\text{forward}}$, $\text{open_list}_{\text{backward}}$,
 $\text{close_list}_{\text{backward}}$, $\mathbf{n}_{\text{start}}$, \mathbf{n}_{goal}

Result: Path from $\mathbf{n}_{\text{start}}$ to \mathbf{n}_{goal}

```

1 Initialize  $\text{open\_list}_{\text{forward}} = \{\}$ ,  $\text{close\_list}_{\text{forward}} = \{\}$ ,  

    $\text{open\_list}_{\text{backward}} = \{\}$ ,  $\text{close\_list}_{\text{backward}} = \{\}$ 
2  $\mathbf{n}_{\text{start}} \rightarrow \text{open\_list}_{\text{forward}}$ 
3  $\mathbf{n}_{\text{goal}} \rightarrow \text{open\_list}_{\text{backward}}$ 
4 while  $\text{open\_list}_{\text{forward}} \neq \{\}$  and  $\text{open\_list}_{\text{backward}} \neq \{\}$  do
5    $\mathbf{n}_{\text{current},f} =$  the node in  $\text{open\_list}_{\text{forward}}$  with the smallest  $f(\mathbf{n})$ 
6    $\mathbf{n}_{\text{current},b} =$  the node in  $\text{open\_list}_{\text{backward}}$  with the smallest  $f(\mathbf{n})$ 
7   if  $\mathbf{n}_{\text{current},f} = \mathbf{n}_{\text{current},b}$  then
8     | return optimal path by connecting  $\mathbf{n}_{\text{current},f}$  and  $\mathbf{n}_{\text{current},b}$ 
9   end
10   $\text{open\_list}_{\text{forward}} \leftarrow \text{open\_list}_{\text{forward}} - \mathbf{n}_{\text{current},f}$ 
11   $\text{close\_list}_{\text{forward}} \leftarrow \text{close\_list}_{\text{forward}} + \mathbf{n}_{\text{current},f}$ 
12   $\text{open\_list}_{\text{backward}} \leftarrow \text{open\_list}_{\text{backward}} - \mathbf{n}_{\text{current},b}$ 
13   $\text{close\_list}_{\text{backward}} \leftarrow \text{close\_list}_{\text{backward}} + \mathbf{n}_{\text{current},b}$ 
14  foreach  $\mathbf{n}_{i,f} \in$  eight neighborhoods of  $\mathbf{n}_{\text{current},f}$  do
15    if  $\mathbf{n}_{i,f} \neq \text{obstacle}$  and  $\mathbf{n}_{i,f} \notin \text{open\_list}_{\text{forward}}$  and  

        $\mathbf{n}_{i,f} \notin \text{close\_list}_{\text{forward}}$  then
16      |  $\mathbf{n}_{i,f} \rightarrow \text{open\_list}_{\text{forward}}$ 
17      |  $\mathbf{n}_{\text{current},f} = \mathbf{n}_{i,\text{parents},f}$ 
18      | calculate  $f(\mathbf{n}_{i,f})$ ,  $g(\mathbf{n}_{i,f})$ , and  $h(\mathbf{n}_{i,f})$ 
19    end
20    if  $\mathbf{n}_{i,f} \in \text{open\_list}_{\text{forward}}$  then
21      | if  $f'(\mathbf{n}_{i,f}) < f(\mathbf{n}_{i,f})$  then
22        | |  $f(\mathbf{n}_{i,f}) = f'(\mathbf{n}_{i,f})$ 
23        | |  $\mathbf{n}_{\text{current},f} = \mathbf{n}_{i,\text{parents},f}$ 
24      end
25    end
26  end
27  foreach  $\mathbf{n}_{i,b} \in$  eight neighborhoods of  $\mathbf{n}_{\text{current},b}$  do
28    if  $\mathbf{n}_{i,b} \neq \text{obstacle}$  and  $\mathbf{n}_{i,b} \notin \text{open\_list}_{\text{backward}}$  and  

        $\mathbf{n}_{i,b} \notin \text{close\_list}_{\text{backward}}$  then
29      |  $\mathbf{n}_{i,b} \rightarrow \text{open\_list}_{\text{backward}}$ 
30      |  $\mathbf{n}_{\text{current},b} = \mathbf{n}_{i,\text{parents},b}$ 
31      | calculate  $f(\mathbf{n}_{i,b})$ ,  $g(\mathbf{n}_{i,b})$ , and  $h(\mathbf{n}_{i,b})$ 
32    end
33    if  $\mathbf{n}_{i,b} \in \text{open\_list}_{\text{backward}}$  then
34      | if  $f'(\mathbf{n}_{i,b}) < f(\mathbf{n}_{i,b})$  then
35        | |  $f(\mathbf{n}_{i,b}) = f'(\mathbf{n}_{i,b})$ 
36        | |  $\mathbf{n}_{\text{current},b} = \mathbf{n}_{i,\text{parents},b}$ 
37      end
38    end
39  end
40 end

```

Algorithm 2. Bidirectional Search A* Algorithm.

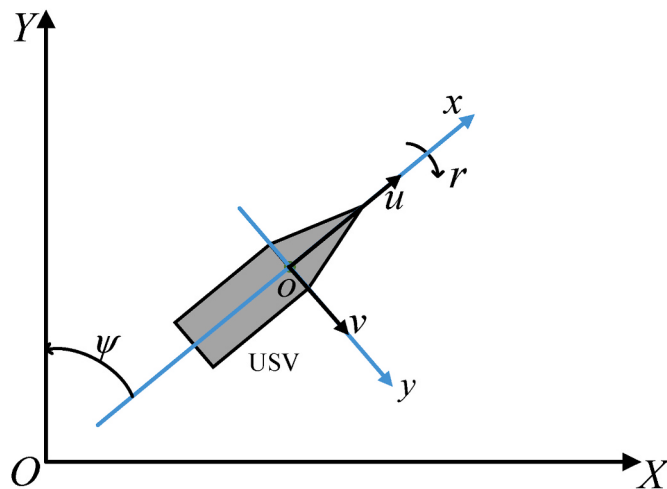


Fig. 2. The description of 3-DOF planar vessel motion variables.

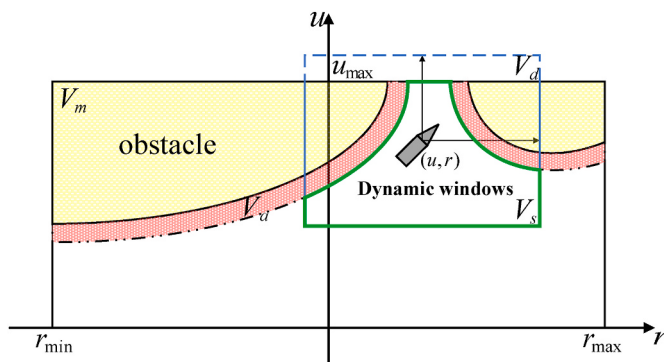


Fig. 3. Schematic of velocity sampling space selection.

3.3. Prediction of the feasible trajectory

After obtaining the velocity sampling space in the above section, it is possible to discretize the feasible velocity pairs (u, r) from this space. To obtain the optimal velocity pairs (u, r) , it is necessary to predict the local path of the USV for each velocity pair within one cycle. If the time step Δt in each period is small enough, the motion velocities of the USV at time $t + \Delta t$ can be calculated with uniform acceleration. Then the surge speed $u(t + \Delta t) = u(t) + \dot{u}(t)\Delta t$ of the USV at $t + \Delta t$, combined with the kinematics Eq. (6) of USV, the velocities in the geocentric inertial coordinate system are obtained:

$$\begin{cases} \dot{x}(t) = u(t)\cos\psi(t) - v(t)\sin\psi(t) \\ \dot{y}(t) = u(t)\sin\psi(t) + v(t)\cos\psi(t) \\ \dot{\psi}(t) = r(t) \end{cases} \quad (11)$$

The position $x(t + \Delta t) = x(t) + \dot{x}(t)\Delta t$ of the USV at $t + \Delta t$, continues the iterative calculation described above through simulation cycles Δt until the USV reaches the target point. As shown in Fig. 4, the green curve represents the feasible predicted trajectory of the USV, the yellow area represents obstacles, and the red pentagram represents the target point.

3.4. Collision risk assessment

In the process of defining the velocity sampling space V_s , the velocity pairs (u, r) linked with the predicted trajectory are discretized within this space. Subsequently, the optimal trajectory and its corresponding optimal velocity set are chosen. Preceding this selection, it is crucial to establish an objective evaluation function aimed at filtering plausible

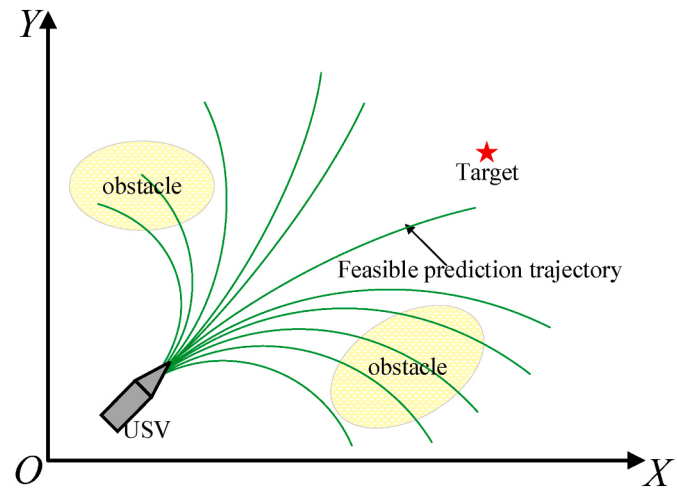


Fig. 4. Schematic of feasible trajectory projections.

predicted trajectories. The evaluation function should encompass the following metrics:

1. To be able to move towards the target point.
2. To be able to move towards the target point while at the same time being fast.
3. Most importantly, to be able to effectively avoid obstacles.

The evaluation function metrics of the DWA algorithm are defined as:

- a. Heading angle evaluation function $Head(u, r)$.

$$Head(u, r) = 180^\circ - \theta \quad (12)$$

In this paper, the global path extraction points are considered temporary target points for the USV. The heading angle evaluation function is used to measure the angular difference θ between the temporary target point and the predicted heading. The magnitude of the angle inversely correlates with the resultant evaluation score, where a smaller angle corresponds to a higher score. As shown in Fig. 5.

- b. Surge speed evaluation function $Vel(u, r)$.

$$Vel(u, r) = u_c \quad (13)$$

$Vel(u, r)$ represents velocity pair (u_c, r_c) . This function is used to evaluate surge speed u during the navigation process of the USV, in order to meet the requirement of the USV moving towards the target point as quickly as possible.

- c. Distance evaluation function $Dist(u, r)$.

$$Dist(u, r) = \begin{cases} c & d_0 > R \\ 0 & d_0 \leq R \end{cases} \quad (14)$$

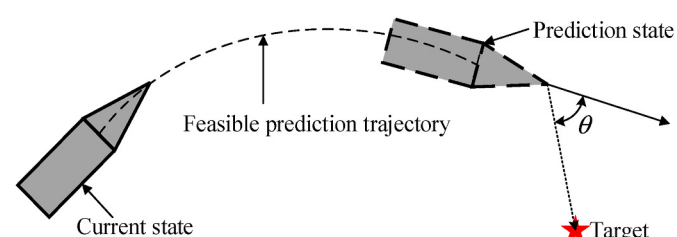


Fig. 5. The description of heading angle function.

According to Szlapczynski et al., it can be learned that the ship domain (Szlapczynski and Szlapczynska, 2017) is generally elliptical, as shown in Fig. 6, where L is the length of the USV and the diameter of the circumscribed circle of the USV model.

where d_0 is the closest distance between the predicted trajectory corresponding to the current velocity set (u_c, r_c) and the obstacles. R is the USV's designated safety radius, $R = 6L$, and c is a constant value. If there are no obstacles encountered by the USV during navigation or $d_0 > R$, then $Dist(u, r)$ is set to a larger constant value c . If $d_0 \leq R$, indicating that the predicted trajectory cannot effectively avoid obstacles, then $Dist(u, r)$ is set to 0, reducing the evaluation score of that predicted trajectory. As shown in Fig. 7.

The Dynamic Window Approach (DWA) acquires a viable set of velocities through the sampling of the velocity space, aligning with the kinematic model. Subsequently, it assesses simulated trajectories within this velocity set during a simulation cycle using an evaluation function. The objective is to identify the optimal predicted trajectory along with its associated velocity set. The initial trajectory evaluation function is expressed as follows:

$$G(u, r) = \sigma[\alpha \cdot Head(u, r) + \beta \cdot Dist(u, r) + \gamma \cdot Vel(u, r)] \quad (15)$$

where α , β and γ are the weighting coefficients for $Head(u, r)$, $Dist(u, r)$ and $Vel(u, r)$ respectively, σ is the smoothing factor.

In addressing the non-uniform magnitudes of the three aforementioned evaluation functions, the normalization process is essential to prevent dominance by a disproportionately large value. Each evaluation sub-function undergoes normalization, as expressed by the following calculation equation:

$$\left\{ \begin{array}{l} \sigma \cdot Head(u, r) = normalize - Head_i(u, r) = \frac{Head_i(u, r)}{\sum_{i=1}^n Head_i(u, r)} \\ \sigma \cdot Dist(u, r) = normalize - Dist_i(u, r) = \frac{Dist_i(u, r)}{\sum_{i=1}^n Dist_i(u, r)} \\ \sigma \cdot Vel(u, r) = normalize - Vel_i(u, r) = \frac{Vel_i(u, r)}{\sum_{i=1}^n Vel_i(u, r)} \end{array} \right. \quad (16)$$

where n is the total number of feasible predicted trajectories within one simulation cycle, and i is the currently evaluated feasible predicted trajectory.

The function $G(u, r)$ can satisfy the basic requirement of the USV to safely reach the target point in a short period. However, considering the potential collision risk of the dynamic obstacles, unknown obstacles, and the collision avoidance rules, it is necessary to modify the evaluation function $G(u, r)$ to make it more suitable for evaluating the USV's collision avoidance behaviour.

d. Collision avoidance rules evaluation function $Colregs(u, r)$.

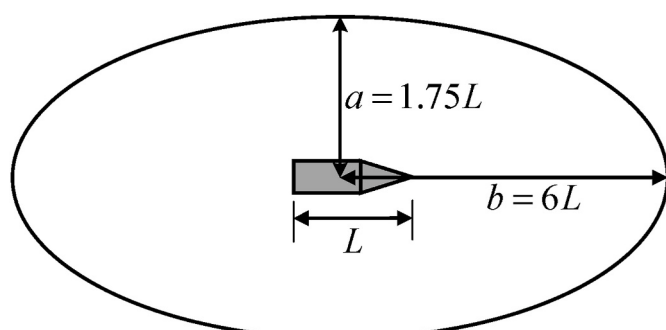


Fig. 6. Elliptical ship domain.

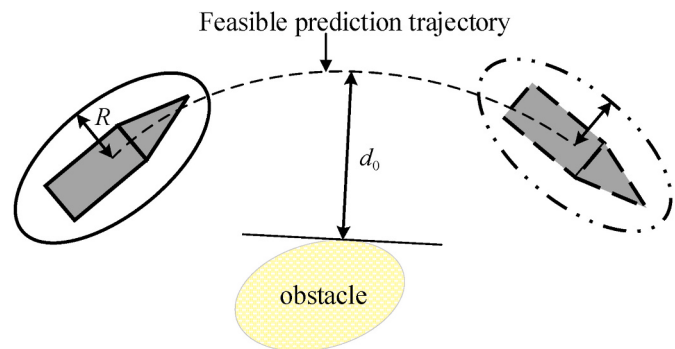


Fig. 7. The description of distance function.

In the LPP process, the USV may encounter moving obstacles such as incoming vessels. In such cases, we consider there to be a collision risk between the two vessels. It is necessary to take evasive actions following the collision avoidance rules based on the encountered situation, to protect the safety of life, property, and the environment. In Articles 13 to 15 of the maritime collision avoidance rules, collision situations are categorized as overtaking, head-on, and crossing situations. By analyzing the research findings of Thyri et al., this paper defines the scope of COLREGs (Thyri et al., 2020), as shown in Fig. 8.

This paper focuses on head-on and crossing encounters. The division and analysis of collision avoidance behaviour using the collision avoidance rules for head-on encounters are as follows:

Head-on situation: When two power-driven vessels are approaching or on opposite courses and there is a risk of collision, both vessels should alter their course to starboard, passing each other from port side to the port side. Specifically, when there is an approaching vessel within the range $\theta_c \in (0^\circ, 15^\circ) \cup (345^\circ, 360^\circ)$, it is encouraged to reward the correct angular velocity that causes our vessel to change its course to starboard.

The right-of-way for crossing starboard vessel situation: When two power-driven vessels are crossing paths and there is a risk of collision, the vessel on the starboard side of the other vessel should give way. If conditions permit, they should also avoid crossing ahead of the other vessel. When $\theta_c \in (15^\circ, 112.5^\circ)$, there is an oncoming vessel from right to left in the starboard forward sector of our vessel. In this case, our vessel should change its course to starboard and pass astern of that vessel. When $\theta_c \in (247.5^\circ, 345^\circ)$ there is an oncoming vessel from left to right in the port forward sector of our vessel. In this case, our vessel should change its course to port and pass astern of that vessel.

According to the analysis of the designed predicted trajectories, when $r_c > 0$, the predicted trajectory tends to concentrate on the port side of the USV. When $r_c < 0$, the predicted trajectory tends to concentrate on the starboard side of the USV. In conclusion, when setting the evaluation function for the USV's predicted trajectory, it is important to reward the correct rate of change of yaw rate. This allows the USV to prioritize selecting action plans that comply with international maritime collision avoidance rules during crossing encounters,

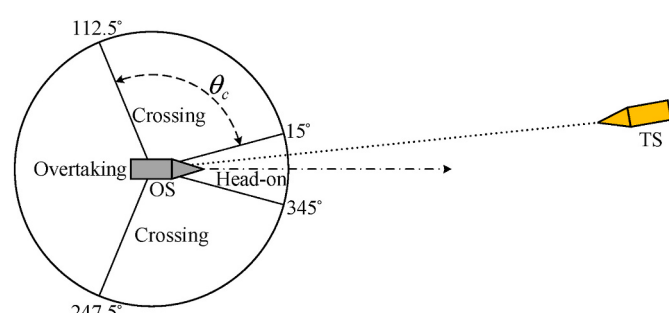


Fig. 8. The division of encounter type.

thereby enhancing navigation safety. Based on the above analysis, the proposed evaluation function is as follows:

$$Colregs(u, r) = \begin{cases} -r_c & \theta_c \in [0^\circ \sim 112.5^\circ] \cup [345^\circ \sim 360^\circ] \\ r_c & \theta_c \in [247.5^\circ \sim 345^\circ] \end{cases} \quad (17)$$

where r_c is the current rate of change of the yaw rate of the USV.

e. Distance to path extraction point evaluation function $Dist_1(u, r)$.

In LPP, sometimes the complexity of the environment can cause the local planned path of the USV to deviate from the global path extraction points (temporary target points), leading to a decrease in the guidance of the global planned path on the local planned path. To address this issue, this paper introduces the distance to path extraction point evaluation function as follows:

$$Dist_1(u, r) = \frac{1}{d_1} \quad (18)$$

where d_1 is the closest distance between the predicted trajectory corresponding to the current velocity set (u_c, r_c) and the path extraction point.

Finally, the trajectory evaluation function can be rewritten as follows:

$$G(u, r) = \sigma \left(\alpha \cdot Head(u, r) + \beta \cdot Dist(u, r) + \gamma \cdot Vel(u, r) \right) + \eta \cdot Colregs(u, r) + \lambda \cdot Dist_1(u, r) \quad (19)$$

The normalization calculation equation for the sub-function are defined as:

$$\sigma \cdot Colregs(u, r) = normalize - Colregs_i(u, r) = \frac{Colregs_i(u, r)}{\sum_{i=1}^n Colregs_i(u, r)} \quad (20)$$

$$\sigma \cdot Dist_1(u, r) = normalize - Dist_{1i}(u, r) = \frac{Dist_{1i}(u, r)}{\sum_{i=1}^n Dist_{1i}(u, r)} \quad (21)$$

4. Hybrid path planning method for USVs

Global Path Planning (GPP) is a technique assuming complete knowledge of the overall environmental layout. The path generated on a global scale directs the navigation of USVs. However, GPP is deficient in real-time information, particularly regarding dynamic obstacles that the USV might encounter or the unforeseen dynamic obstacles obstructing the predetermined global path. For real-time path planning in dynamic environments, Local Path Planning (LPP) with Dynamic Window Approach (DWA) proves effective. Nevertheless, owing to the algorithm's dependence on prior data and the intricacies of the surroundings, it is susceptible to becoming ensnared in local optima, significantly compromising the safe navigation of the USV. Moreover, from an energy consumption standpoint, the absence of guidance from the globally planned path to the locally planned path often results in deviations, distancing the local path from the globally optimal route. This invariably leads to a certain level of energy inefficiency.

This study augments both the bidirectional A* algorithm and DWA within the context of path planning for USVs. The proposed dynamic path planning algorithm operates as follows: the USV adheres to the globally shortest path determined by the bidirectional A* algorithm, while continually monitoring environmental changes. Upon detecting an impending environmental change, the USV transitions to the improved DWA algorithm customized for the specific conditions of Local Path Planning (LPP). Following obstacle avoidance, the USV reverts to the global path to resume its journey. The algorithm process is as follows:

Step 1: The pertinent area for path planning is derived from the electronic nautical chart. Grayscale and rasterization techniques are applied to this chart region to serve as the global environment for path planning. The initial and target points for the Unmanned Surface Vehicle (USV) are established within this global environment.

Step 2: Use an improved A* algorithm for GPP to search the globally optimal path.

Step 3: Dynamic obstacles that may encounter the USV and unknown obstacles obstructing the USV's navigation route are placed along the generated global path.

Step 4: Set the various parameters for LPP and select a path extraction point from the generated global path at regular intervals as the temporary target point for LPP.

Step 5: Generate feasible predicted trajectories within one simulation cycle under the constraints of the velocity sampling space.

Step 6: Detect the environmental information around the USV.

Step 7: Evaluate the predicted trajectories using the environmental information with the defined evaluation function to guide the USV.

Step 8: Check if the USV has reached the temporary target point. If not, continue the execution of the algorithm until the USV reaches the temporary target point.

Continuously update the subsequent temporary target point until the USV arrives at the target point. The flow structure of the algorithm is illustrated in Fig. 9.

5. Simulation tests

This section focuses on the validation of the proposed hybrid dynamic path planning algorithm in complex environments considering dynamic and unknown obstacles, as well as COLREGs rule.

5.1. Comparative study of the proposed bidirectional A* algorithm

Firstly, the simulation test was carried out to validate the performance of the proposed bidirectional A* algorithm in this paper. The results (path length, running time, and number of turning corners) are compared with the traditional A* algorithm. As shown in Fig. 10 and (a) shows the result of global path planning using the A* algorithm and Fig. 10(b) shows the result of global path planning using the proposed bidirectional A* algorithm. The blue area represents the search trace of the forward search, the yellow area represents the search trace of the backward search, and the red trajectory corresponds to the globally planned path. Table 1 gives a comparison of the path length, average running time, and number of turning corners for the two algorithms.

From Tables 1, it can be observed that the bidirectional A* algorithm reduces its average running time by 52.52%, although the path length and the number of turning corners do not change significantly. The efficiency is significantly improved by using the bidirectional A* algorithm.

5.2. Comparative study of the collision avoidance algorithms

To assess the efficacy of the proposed collision avoidance algorithm, a simplified simulation case, depicted in Fig. 11–Fig. 14 was used for the validation. Throughout the simulation, the Dynamic Window Approach (DWA) collision avoidance algorithm is denoted as DCA. Additionally, the COLREGs-based DWA collision avoidance algorithm proposed in this study is abbreviated as CDCA. The simulation scenario comprises randomly positioned static obstacles, USVs, and approaching vessels, with the speed of the incoming vessels uniformly set to 1 m/s.

The interaction between incoming vessels and the USV emulates a Crossing encounter situation and a Head-on situation, respectively. This setup aims to verify the collision avoidance effectiveness of CDCA on moving obstacles. Furthermore, it assesses the impact of the evaluation function, grounded in the constraints of collision avoidance rules, on the

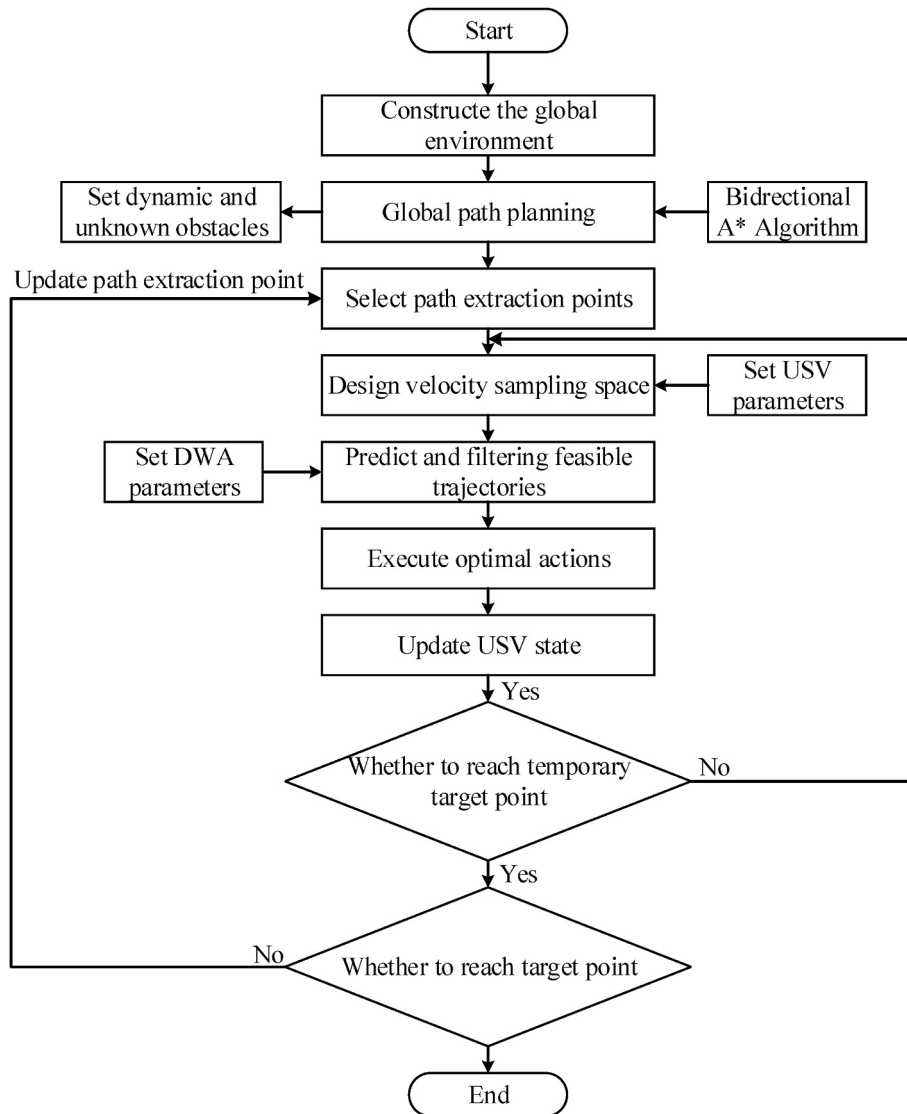


Fig. 9. Flow chart of the proposed hybrid path planning algorithm.

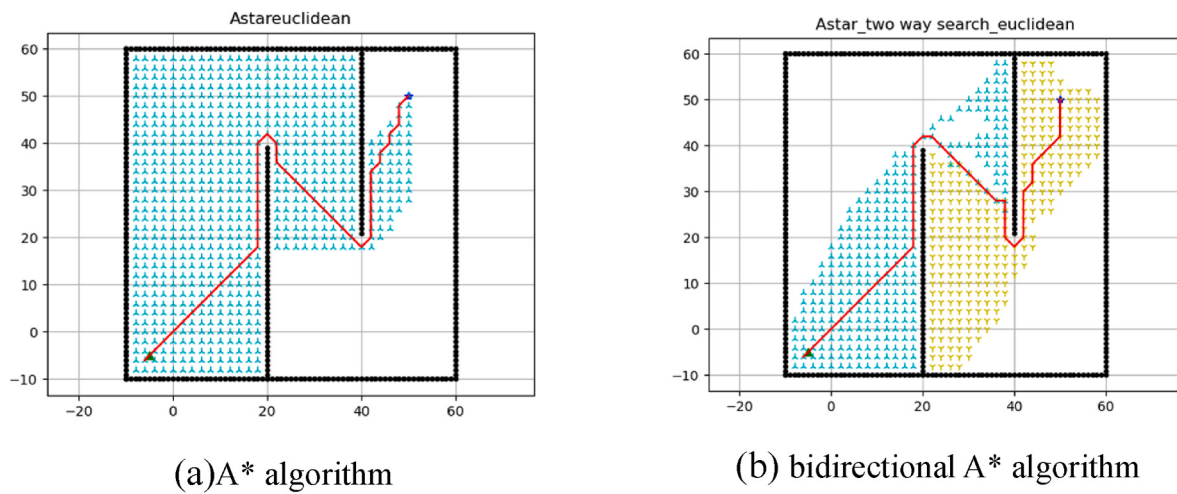


Fig. 10. Comparison graph of search strategy optimization.

Table 1

Comparison of results for various parameters of the optimized algorithm.

algorithm	path length	running time	turning corner
A* algorithm	63.5979	5.4089	14
bidirectional A* algorithm	64.7656	2.5681	14

collision avoidance outcomes. **Table 2** displays the configured weighted coefficient parameters for both DCA and CDCA.

The collision avoidance outcomes for Dynamic Collision Avoidance (DCA) in both Crossing and Heading-on situations are illustrated in **Figs. 11 and 13**, respectively. Correspondingly, the collision avoidance results for Cooperative Dynamic Collision Avoidance (CDCA) in Crossing and Heading-on situations are presented in **Figs. 12 and 14** respectively.

According to the simulation results, as given in **Fig. 11**, the hybrid dynamic path planning algorithm utilizing DCA successfully navigates around a moving obstacle ship in a Crossing situation. However, it tends to converge to a local optimum in complex environments containing both static and dynamic obstacles, as illustrated in **Fig. 11(d)**. This behaviour causes the USV to adhere to static obstacles, compromising collision avoidance safety. In **Fig. 13(b)**, the USV effectively avoids a moving obstacle ship and reaches the target point in a Heading-on situation. Nevertheless, it passes on the starboard side of the obstacle ship, as revealed in **Fig. 13(c)**, violating the COLREGs.

In **Fig. 12(c)**, the hybrid dynamic path planning algorithm using CDCA, proposed in this paper, not only avoids an obstacle ship in a Crossing situation but also ensures that the USV passes from the left side and stern of the ship, meeting the COLREGs for collision avoidance, as shown in **Fig. 12(d)**. Simultaneously, an evaluation subfunction

$Dist_1(u, r)$ is incorporated to prevent the USV from falling into a local optimum during dynamic obstacle avoidance. **Fig. 14(b)** illustrates that the USV successfully avoids an incoming ship in a Heading-on situation and, importantly, passes through the port side of the obstacle ship, as shown in **Fig. 14(c)**. This collision avoidance operation adheres to the COLREGs, providing comprehensive navigation safety assurance.

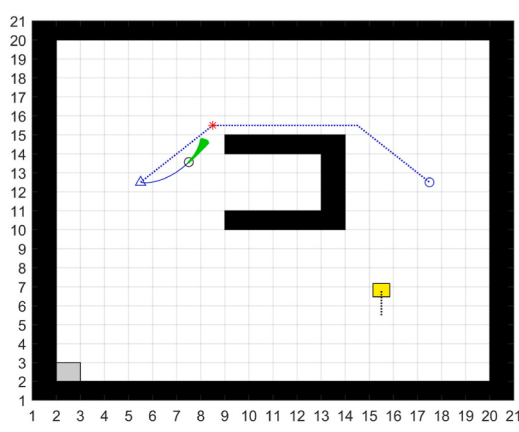
5.3. Simulation tests in the real environment

The designated test location is the coastal area of Zhoushan City in southeastern Zhejiang Province, China, encompassing multiple islands, as illustrated in **Fig. 15(a)**, making it an optimal region for path planning. To facilitate subsequent rasterization processing, the map of the Zhoushan Archipelago is processed with grayscale. The grayscale map is then converted into a matrix consisting of 0 and 1, where 0 represents navigable waters and 1 represents non-navigable areas. A trade-off exists between the calculation time of the path planning algorithm and the resolution of the grid map. This is because higher resolutions inherently demand longer computation time. Consequently, it becomes essential to carefully select an acceptable size for each grid cell during rasterization. Considering manoeuvrability standards for vessels, where the minimum turning radius for small vessels is three times their length, and the actual

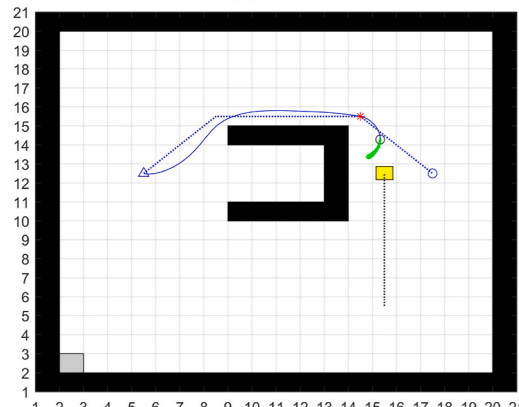
Table 2

Weighted coefficient parameters corresponding to DCA and CDCA.

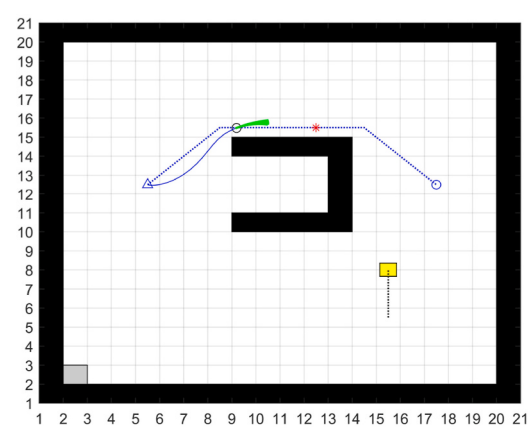
algorithm	α	β	γ	η	λ
DCA	0.05	0.25	0.2	\	\
CDCA	0.05	0.25	0.2	0.15	0.2



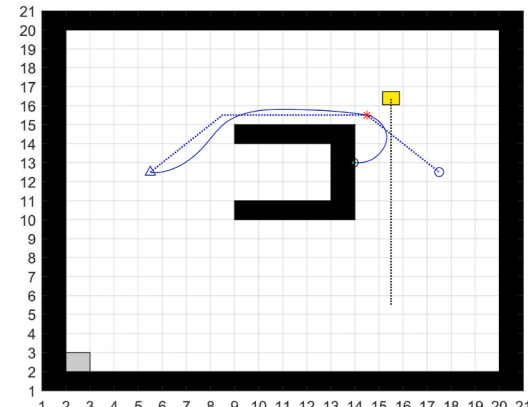
(a)29s



(c)98s



(b)46s



(d)160s

Fig. 11. Crossing situation test using DCA.

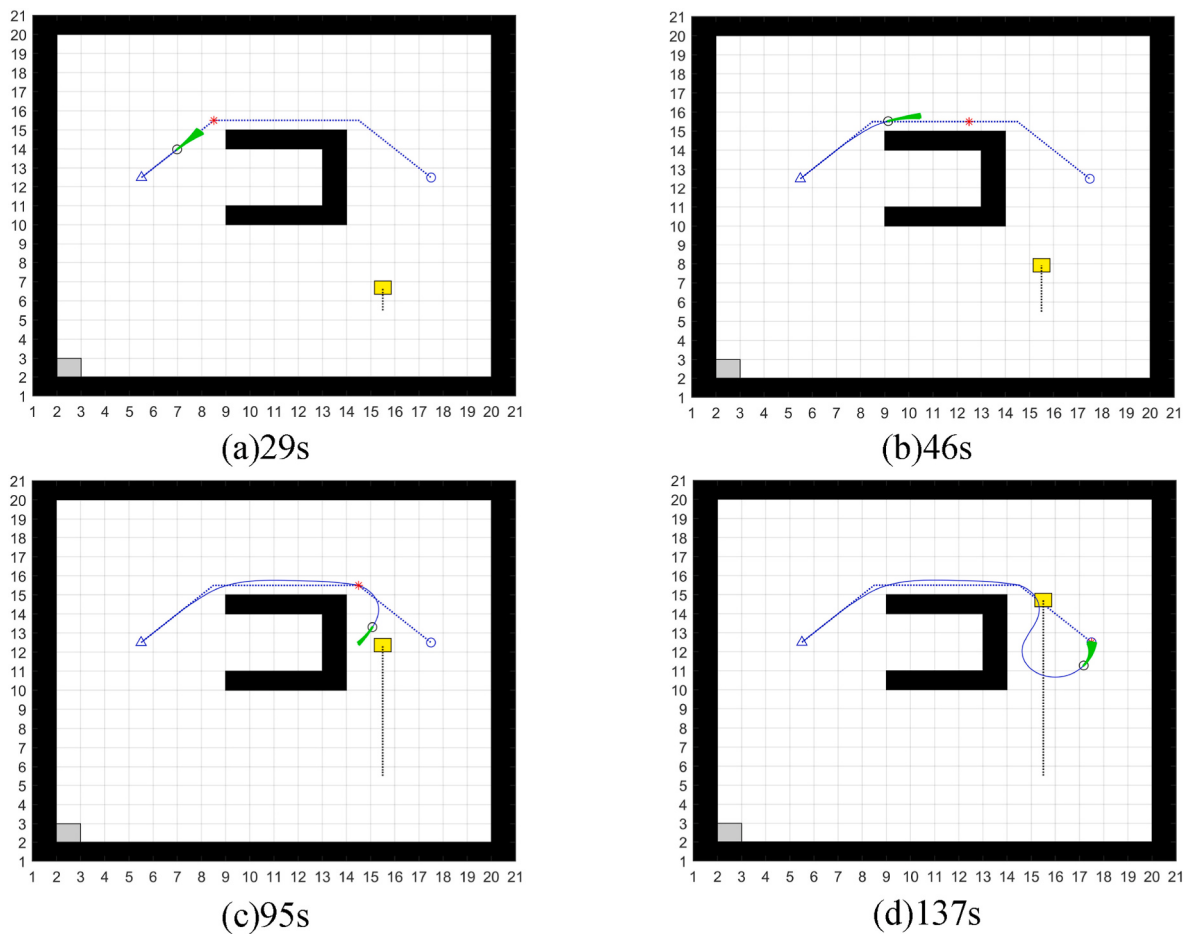


Fig. 12. Crossing situation test using CDCA.

size of the Zhoushan Archipelago map, this paper sets the size of each grid cell to $26.24\text{m} \times 11.48\text{m}$, totalling 100×100 cells, as shown in Fig. 15(b). With this configuration, the USV will be able to manoeuvre flexibly within each grid cell by turning left or right.

In the simulation, the parameters of the USV are set as shown in [Table 3](#). Since the size of the USV is much smaller than the grid cell, so, it can be treated as a point in the article and its safety radius is displayed. The start point of the USV is selected as $S = [29, 42]$, and the target point of the USV is selected as $G = [86, 77]$, as shown in [Fig. 16](#).

Given the environmental map, starting point, and target point, the global path can be generated based on the previously mentioned global path planning algorithm, as shown in Fig. 16. The blue dashed line in the figure is the USV's global planned path, which is the planned trajectory of the USV. According to the characteristics of the global path planning algorithm, this path is the shortest distance from the starting point to the target point. In the grid-processed map, it can be observed that the global path sometimes gets very close to the edges of islands. This is one of the drawbacks of global path planning algorithms, as they often prioritize optimality and overlook the important issue of path safety.

To verify the adaptability of the algorithm in complex environments, this paper incorporated unknown obstacles and dynamic obstacles into the global environment. Additionally, to evaluate the effectiveness of the proposed collision avoidance rule evaluation function, dynamic obstacles were set to intersect with the USV's planned path. Two unknown obstacles were temporarily placed on the USV's path, and their location information is shown in [Table 4](#). Set up a dynamic obstacle moving at a constant speed of 0.32 m/s, as shown in [Fig. 17\(a\)](#). The black triangle represents the starting point of the dynamic obstacle, and the black circle represents its target point. The red solid line represents

the predefined trajectory of the dynamic obstacle, which intersects with the global planned path mentioned earlier to simulate the USV's encounter with other vessels. The grey rectangle represents an unknown obstacle that obstructs the USV's global planned path. Set the parameters in the evaluation function for the predicted trajectory, as shown in [Table 5](#). The prediction time is to be set to 2.0s simultaneously. With this, the construction of the global environment in this paper is completed, and a complex environment is further constructed on top of it to verify the applicability of the algorithm.

Fig. 17 illustrates the comprehensive procedure of the proposed hybrid dynamic path planning algorithm. At the initial moment (0s), is used to plan the global path of the USV based on the global environment, considering the global environment, starting points, and the destination. Concurrently, the first path extraction point is designated on the global path, serving as a provisional target point to guide the local path planning for the USV. A dynamic obstacle, representing an approaching vessel, is introduced, commencing its trajectory from the starting point and advancing towards the target point at a velocity of 0.32 m/s. An unforeseen obstacle materializes on the global path, impeding the USV's trajectory, as depicted in **Fig. 17(a)**. In **Fig. 18**, at 2s, the USV exhibits a surge speed of 0.02 m/s, a yaw rate of -0.087 rad/s, and an attitude angle (defined as the angle between the heading of the USV and the x-axis of the map coordinate system).

At 216s, The USV starts to encounter the simulated oncoming vessel. According to the COLREGs, at this moment the USV should alter its course to starboard and pass astern of the oncoming vessel, as shown in Fig. 17(c). In Fig. 18, during the period 216s–251s, the surge speed of the USV decreases from 0.62 m/s to 0.48 m/s, indicating that the USV decelerates to ensure safe navigation when encountering the oncoming

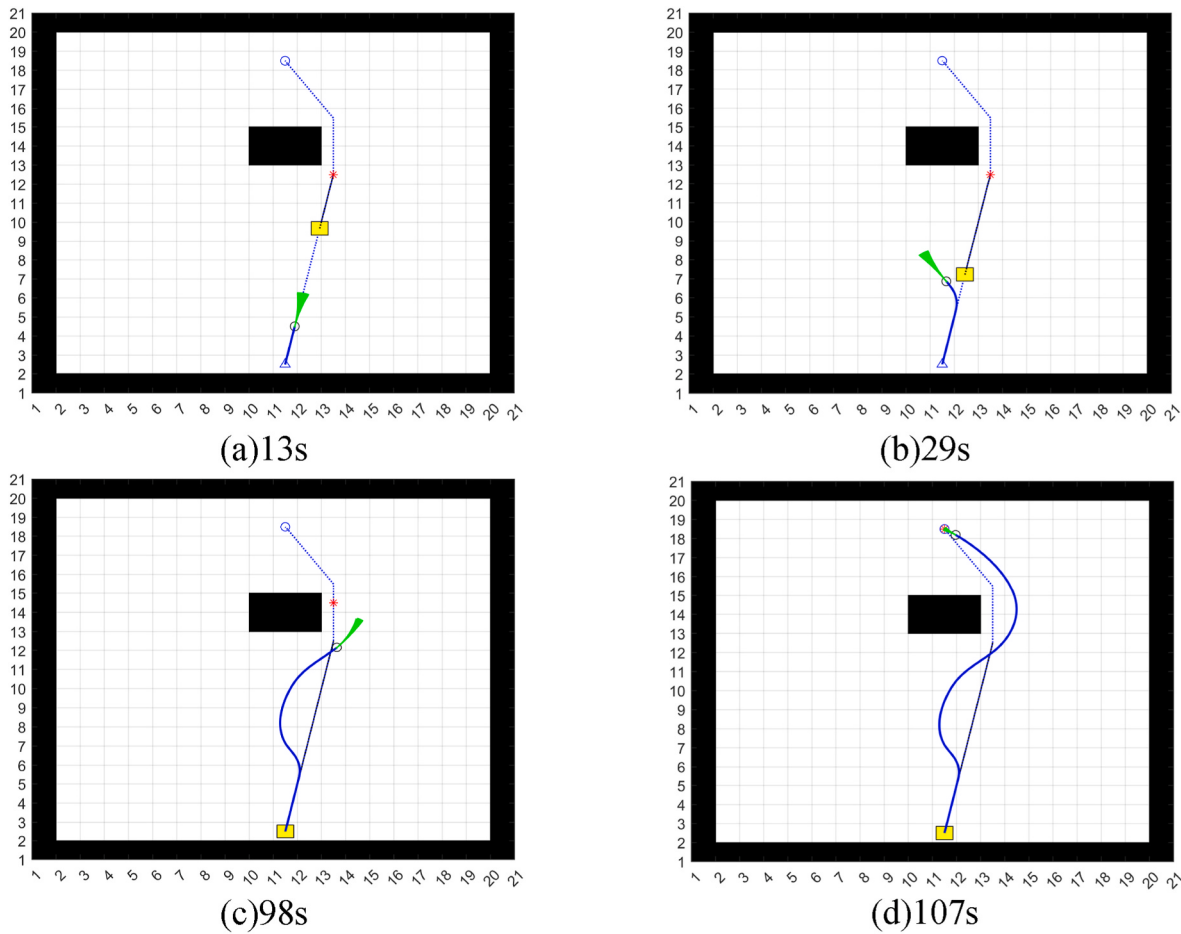


Fig. 13. Heading-on situation test using DCA.

vessel. The yaw rate of the USV decreases from 0 rad/s to -0.349 rad/s, indicating that the USV follows the International Regulations for Preventing Collisions at Sea and alters its course to portside when encountering the oncoming vessel. At 284s, the attitude angle of the USV is -82.2° . It can be expected the USV will collide with moving obstacles if the path planning system does not consider the dynamic obstacles and COLREGs rules.

At 396s, the USV manoeuvres around the oncoming vessel and continues along the global path. Combined with Fig. 18, the surge speed of the USV returns to 0.62 m/s, the yaw rate is 0.105 rad/s, and the attitude angle is -30.7° .

At 920s, the USV is about to approach a corner of the global path. As mentioned above, the planned path at the region is too close to the obstacle, which is dangerous for the navigation process of the USV. With the aid of the LPP and the defined safe radius for the USV, the USV deviates to a certain extent from the global path, which ensures the safe navigation of the USV, as shown in Fig. 17(d). In Fig. 18, at 920s, the surge speed of the USV remains unchanged, and the yaw rate decreases from 0 rad/s to -0.192 rad/s. The attitude angle of the USV changes from -38.1° to -43.6° . If the USV were to navigate along the global path, its attitude angle would be -38.1° . This also indicates that by incorporating the local path planning algorithm, unsafe segments of the global path can be corrected and adjusted.

At 2068s, the USV continues to navigate towards the target point and encounters an unknown obstacle 1 obstructing the global path. At this moment, the USV performs avoidance actions on the unknown obstacle 1 that appears on the travel route, as shown in Fig. 17(e). From Fig. 18, during the period 1980s–2068s, the USV's surge speed decreases from 0.62 m/s to 0.56 m/s and then increases again to 0.62 m/s. The yaw rate

increases from 0 rad/s to 0.349 rad/s and then decreases to 0.052 rad/s. The attitude angle changes from 66.1° to 114.7° , which indicates that the USV makes avoidance actions for unknown obstacle 1.

At 3122s, the USV encounters an unknown obstacle 2 obstructing the global path and performs avoidance actions on it, as shown in Fig. 17(f). From Fig. 18, during the period 3028s–3122s, the USV's surge speed decreases from 0.62 m/s to 0.58 m/s and then increases again to 0.62 m/s. The yaw rate decreases from 0 rad/s to -0.349 rad/s and then increases to -0.017 rad/s. The attitude angle changes from 64° to 18.3° , which shows that the USV makes avoidance actions for unknown obstacle 2.

Finally, the USV reaches the target point as shown in Fig. 17(b). At this point, the path planning process of the USV using the hybrid dynamic path planning algorithm concludes.

6. Conclusions

This paper proposes a novel hybrid dynamic path planning algorithm that integrates the Bidirectional A* algorithm and the enhanced DWA algorithm. This amalgamation empowers USVs to autonomously execute path planning and collision avoidance manoeuvres within intricate and dynamically simulated marine environments. The distinct contributions of this research are delineated as follows.

- (1). Global path planning is less responsive to the dynamic environment. This situation may result in outdated or ineffective paths when the environment changes. To tackle this challenge, the local path planning algorithms have been integrated into this paper. This integration facilitates fast responses to environmental

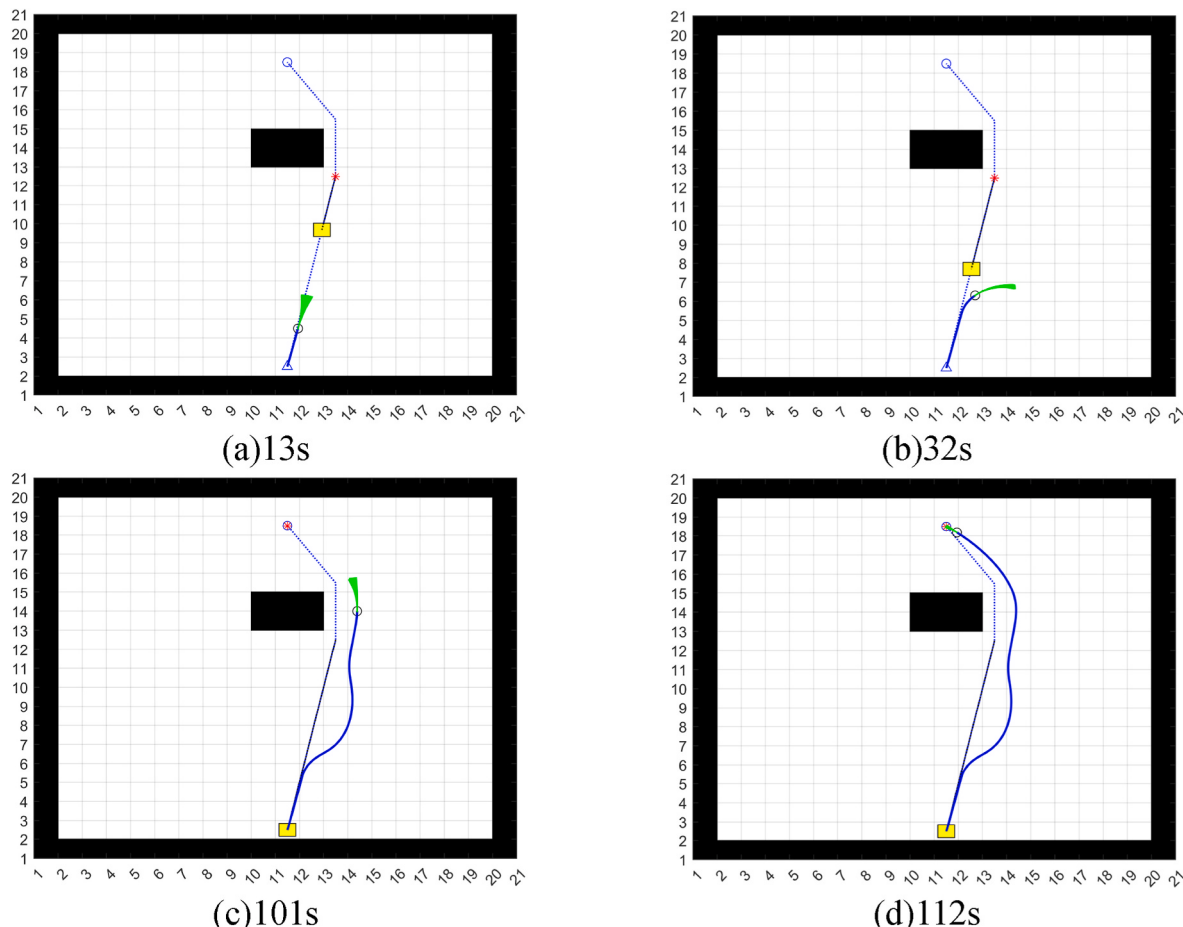


Fig. 14. Heading-on situation test using CDCA.



Fig. 15. Selection and construction of the global environment.

Table 3
Parameter information of the USV.

parameter	value
maximum/minimum surge speed	1.5/0 m/s
maximum/minimum yaw rate	0.3491/-0.3491 rad/s
maximum surge speed acceleration	0.2 m/s ²
maximum yaw rate acceleration	0.8727 rad/s ²
surge speed resolution	0.02 m/s
yaw rate resolution	0.0175 rad/s
initial heading angle	120°

changes and enables real-time adjustments and corrections at a local level. This enhancement leverages the strengths of both global and local approaches, resulting in improved real-time responsiveness, path quality, and safety within the context of path planning.

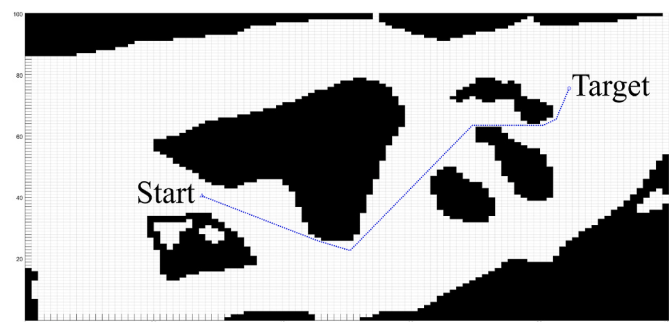


Fig. 16. Global planned path in the global rasterized map.

Table 4

The position of the obstacles.

unknow obstacle	moving obstacle		
unknow obstacle1	(59,42)	start point	(37,34)
unknow obstacle2	(68,59)	end point	(32,42)

- (2). The conventional A* algorithm typically determines the optimal path only when the current search node reaches the destination. This approach often leads to suboptimal path planning efficiency.

To address this issue, this paper adopts a bidirectional search strategy, simultaneously exploring paths from both the starting and target points toward each other. When these searches converge at an intermediate node, the globally optimal path

Table 5

Parameter of the defined evaluation function.

α	β	γ	η	λ
0.05	0.2	0.3	0.15	0.2

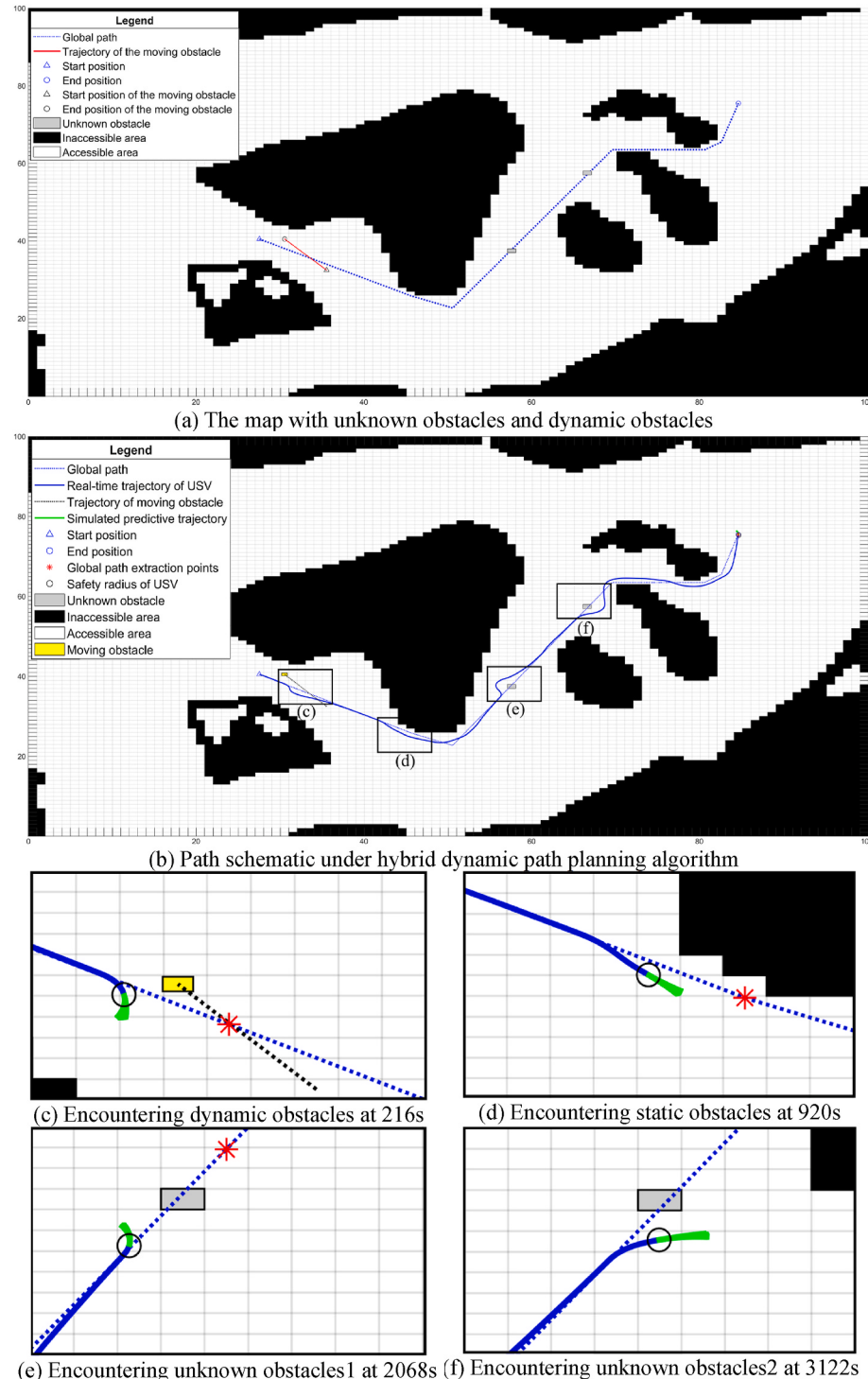


Fig. 17. Simulation process of planning path under hybrid dynamic path planning algorithm.

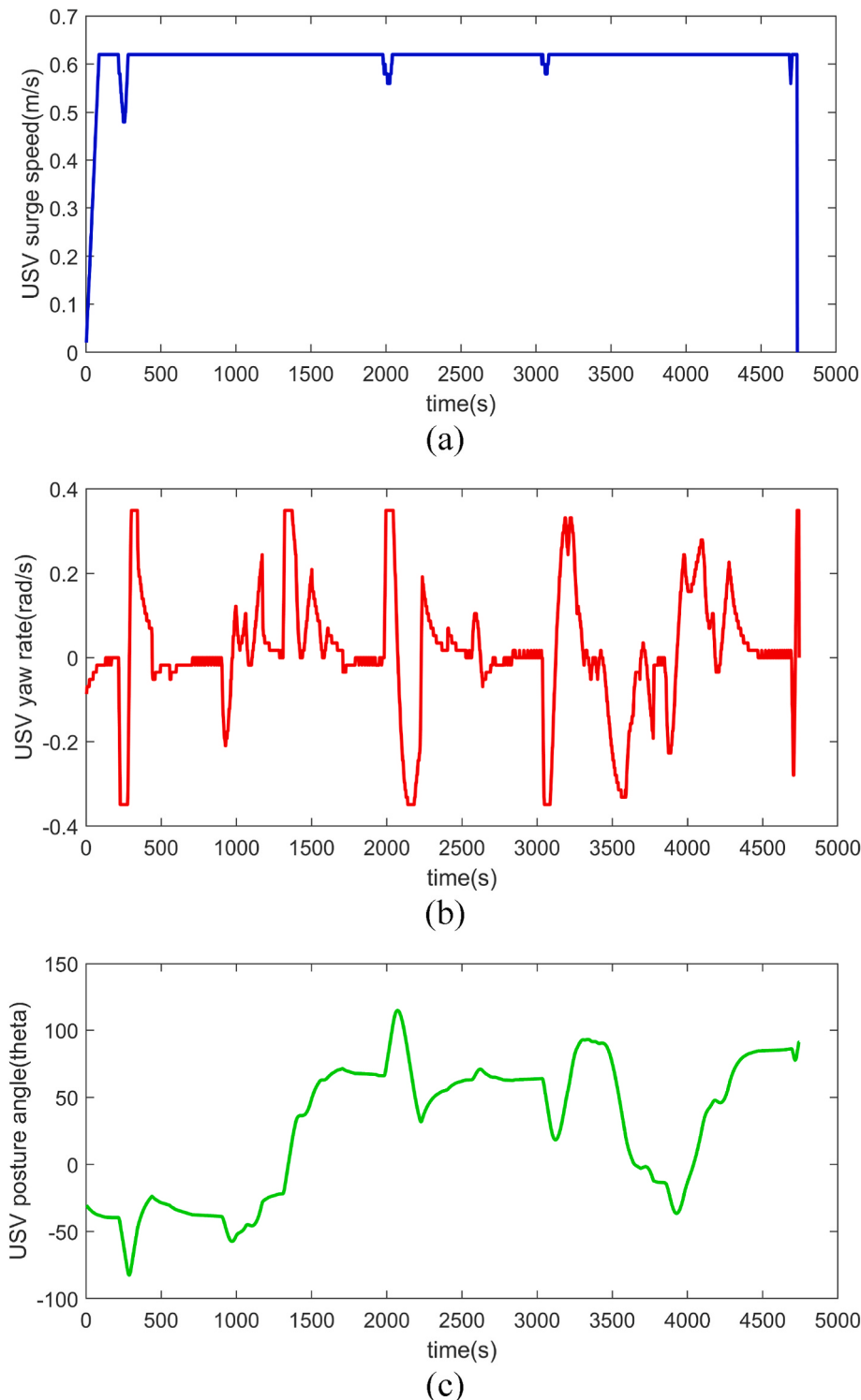


Fig. 18. Time-varying curves of various parameters of the USV. (a) USV surge speed; (b) USV yaw rate; (c) USV posture angle.

becomes accessible. This refinement significantly reduces the search space, enhancing both the efficiency and speed of path planning. Consequently, the algorithm accelerates its ability to generate the globally optimal path.

- (3). This paper presents a novel evaluation function tailored to the extraction points along the global path. Meanwhile, the manoeuvrability, propulsion, and collision risk with static and dynamic obstacles and COLREGs rule are considered in this function. The purpose of this function is to precisely evaluate the

quality of predicted trajectories, directing the algorithm toward globally optimal directions. This enhancement ensures the algorithm's capability to identify feasible paths, even when confronted with intricate obstacles, without succumbing to confinement within local optima.

- (4). By incorporating the international maritime collision avoidance rules as an evaluation function in the DWA algorithm, the USV prioritizes selecting action plans that comply with the rules during the path planning process. It also determines the

interaction approach with other vessels based on these rules, thus avoiding potential collision risks, and improving overall traffic efficiency. This enables the hybrid dynamic path planning algorithm to better adapt to complex and dynamic water environments.

From the simulation tests, the proposed algorithm can reduce the planning time with a higher efficiency, ranging from 53% to 70%. The improved DWA algorithm markedly enhanced the ability of the predicted trajectory to adhere closely to global path extraction points, resulting in a finer alignment between the locally planned path and the globally optimal route. Furthermore, it aids the USV to avoid unknown obstacles and moving vessels, these findings confirm the efficiency, robustness, and safety of the proposed hybrid path planning approach. It is also worth noting that environmental disturbances, such as currents, waves, and wind, play an important role in path planning, particularly for large commercial ships. Moreover, the construction of the simulation environment did not take into account the complex scenarios involving multiple-ship encounters. These challenging issues need to be addressed in further research.

CRediT authorship contribution statement

Donghao Xu: Writing – review & editing, Supervision, Methodology, Funding acquisition, Conceptualization. **Jie Yang:** Writing – review & editing, Writing – original draft, Visualization, Validation, Software, Methodology, Investigation, Formal analysis. **Xueqian Zhou:** Writing – review & editing, Methodology. **Haitong Xu:** Writing – review & editing, Writing – original draft, Visualization, Validation, Supervision, Methodology, Funding acquisition, Conceptualization.

Declaration of competing interest

The authors declare that they have no known competing financial interests or personal relationships that could have appeared to influence the work reported in this paper.

Data availability

Data will be made available on request.

Acknowledgements

We would like to acknowledge the financial support by the Science Fund Project of Heilongjiang Province (LH2021E087). This work was performed within the Strategic Research Plan of the Centre for Marine Technology and Ocean Engineering, financed by the Portuguese Foundation for Science and Technology (Fundação para a Ciência e Tecnologia—FCT) under contract UIDB/UIDP/00134/2020.

Appendix A. Supplementary data

Supplementary data to this article can be found online at <https://doi.org/10.1016/j.oceaneng.2024.117210>.

References

- Berg, J.v.d., Lin, M., Manocha, D., 2008. Reciprocal Velocity Obstacles for Real-Time Multi-Agent Navigation. 2008 IEEE International Conference on Robotics and Automation, pp. 1928–1935.
- Cai, Q., Li, F., 2022. Development Status and Trend of Autonomous Operation for Unmanned Surface Vehicle. Jiangsu Automation Research Institute (China), pp. 2–4.
- Chen, S.J., Huang, J., Miao, H.F., Cai, Y.Q., Wen, Y.Q., Xiao, C.S., 2023. Deep visual waterline detection for inland marine unmanned surface vehicles. *Appl. Sci.* 13 (5), 1–21.
- Dustin J. W., Berg, J.V.D., 2013. Kinodynamic RRT*: Asymptotically Optimal Motion Planning for Robots with Linear Dynamics. IEEE International Conference on Robotics and Automation (ICRA), Karlsruhe, GERMANY, pp. 5054–5061.
- Er, M.J., Li, C., Li, Q., 2021. Hybrid Adaptive Path Planning for a USV under Complex Marine Environment, 2021 4th International Conference on Intelligent Autonomous Systems (ICOIAS), pp. 378–384.
- Er, M.J., Ma, C., Liu, T.H., Gong, H.B., 2023. Intelligent motion control of unmanned surface vehicles: a critical review. *Ocean Eng.* 280, 114562.
- Fernando, S., Laura V. A., Robert C. R., 2023. An unmanned surface vehicle (USV): development of an autonomous boat with a sensor integration system for bathymetric surveys. *Sensors* 23 (9), 4420.
- Fossen, T.I., 2011. Motion Control, Handbook of Marine Craft Hydrodynamics and Motion Control, pp. 227–239.
- Fox, D., Burgard, W., Thrun, S., 1997. The dynamic window approach to collision avoidance. *IEEE Robot. Autom. Mag.* 4 (1), 23–33.
- Fu, M.Y., Wang, S.S., Wang, Y.H., 2019. Multi-behavior fusion based potential field method for path planning of unmanned surface vessel. *China Ocean Eng.* 33 (5), 583–592.
- Gammell, J.D., Srinivasa, S.S., Barfoot, T.D., 2014. Informed RRT*: Optimal Sampling-Based Path Planning Focused via Direct Sampling of an Admissible Ellipsoidal Heuristic. IEEE/RSJ International Conference on Intelligent Robots and Systems (IROS), Chicago, IL, pp. 2997–3004.
- Hao, B., Hao, H., Yan, Z.P., 2023. A path planning approach for unmanned surface vehicles based on dynamic and fast Q-learning. *Ocean Eng.* 270, 113632.
- Hart, P.E., Nilsson, N.J., Raphael, B., 1968. A formal basis for the heuristic determination of minimum cost paths. *IEEE Trans. Syst. Sci. Cybern.* 4 (2), 100–107.
- Hinostroza, M.A., Xu, H.T., Guedes Soares, C., 2018. Path-planning and path-following control system for autonomous surface vessel. In: Teixeir, A.P. (Ed.), Maritime Transportation and Harvesting of Sea Resources, Guedes Soares. Taylor & Francis Group, London, UK, pp. 991–998.
- Hinostroza, M.A., Xu, H.T., Guedes Soares, C., 2019. Cooperative operation of autonomous surface vehicles for maintaining formation in complex marine environment. *Ocean Eng.* 183, 132–154.
- Hinostroza, M.A., Xu, H.T., Guedes Soares, C., 2021. Experimental results of the cooperative operation of autonomous surface vehicles navigating in complex marine environment. *Ocean Eng.* 219, 108256.
- Hosseini, M., Hamid, J., Hamid, A., Elham, O., Farshid, M., Mohammad reza, A., Aref, M. A., Ali, K., Yousef, S.Z., Ashkan, M., 2018. Developing a navigation, guidance and obstacle avoidance algorithm for an Unmanned Surface Vehicle (USV) by algorithms fusion. *Ocean Eng.* 159, 56–65.
- Khatib, O., 1986. The Potential Field Approach And Operational Space Formulation In Robot Control. *Adaptive and Learning Systems: Theory and Applications*. Springer US, Boston, MA, pp. 367–377.
- Kim, H.G., Yun, S.J., Choi, Y.H., Ryu, J.K., Suh, J.H., 2021. Collision avoidance algorithm based on COLREGS for unmanned surface vehicle. *J. Mar. Sci. Eng.* 9 (8), 863.
- Kuffner, J.J., LaValle, S.M., 2000. RRT-connect: An efficient approach to single-query path planning. Proceedings 2000 ICRA. Millennium Conference. IEEE Int. Conf. Robot. Autom. Symp. Proc. 995–1001.
- Liang, C.L., Zhang, X.K., Watanabe, Y., Deng, Y.J., 2021. Autonomous collision avoidance of unmanned surface vehicles based on improved A star and minimum course alteration algorithms. *Appl. Ocean Res.* 113, 102755.
- Liu, Z., Guedes Soares, C., 2023. Sensitivity analysis of a numerical model of the dynamics of gravity cages subjected to current and waves. *Ocean Eng.* 287, 115715. <https://doi.org/10.1016/j.oceaneng.2023.115715>.
- Liu, Z., Guedes Soares, C., 2024. Numerical study of rope materials of the mooring system for gravity cages. *Ocean Eng.* 2024, 11713. <https://doi.org/10.1016/j.oceaneng.2024.117135>.
- Lyu, H.G., Yin, Y., 2019. COLREGS-Constrained real-time path planning for autonomous ships using modified artificial potential fields. *J. Navig.* 72 (3), 588–608.
- Mao, S.Q., Yang, P., Gao, D.J., Bao, C.T., Wang, Z.Y., 2023. A motion planning method for unmanned surface vehicle based on improved RRT algorithm. *J. Mar. Sci. Eng.* 11 (4), 687.
- Shi, B.H., Su, Y.X., Wang, C., Wan, L.L., Luo, Y., 2019. Study on intelligent collision avoidance and recovery path planning system for the waterjet-propelled unmanned surface vehicle. *Ocean Eng.* 182, 489–498.
- Song, R., Liu, Y.C., Bucknall, R., 2019. Smoothed A* algorithm for practical unmanned surface vehicle path planning. *Appl. Ocean Res.* 83, 9–20.
- Sun, X.J., Wang, G.F., Fan, Y.S., Mu, D.D., 2023. Collision avoidance control for unmanned surface vehicle with COLREGS compliance. *Ocean Eng.* 267, 113263.
- Sun, Y.H., Fang, M., Su, Y.X., 2021. AGV path planning based on improved Dijkstra algorithm. *J. Phys. Conf.* 1746 (1), 012052.
- Szlapczynski, R., Szlapczynska, J., 2017. Review of ship safety domains: models and applications. *Ocean Eng.* 145, 277–289.
- Tang, P.P., Zhang, R.B., Liu, D.L., Huang, L.H., Liu, G.Q., Deng, T.Q., 2015. Local reactive obstacle avoidance approach for high-speed unmanned surface vehicle. *Ocean Eng.* 106, 128–140.
- Thyri, E.H., Basso, E.A., Breivik, M., Pettersen, K.Y., Skjetne, R., Lekkas, A.M., 2020. Reactive Collision Avoidance for ASVs Based on Control Barrier Functions. 2020 IEEE Conference on Control Technology and Applications (CCTA), pp. 380–387.
- Wang, Z.Y., Liang, Y., Gong, C.W., Zhou, Y.C., Zeng, C., Zhu, S.L., 2022. Improved dynamit window approach for unmanned surface vehicles' local path planning considering the impact of environmental factors. *Sensors* 22 (14), 5181.
- Xing, B.W., Yu, M.J., Liu, Z.C., Tan, Y.C., Sun, Y., Li, B., 2023. A review of path planning for unmanned surface vehicles. *J. Mar. Sci. Eng.* 11 (8), 1556.
- Xu, H.T., Guedes Soares, C., 2016. Waypoint-following for a Marine Surface Ship Model Based on Vector Field Guidance Law. In: Guedes Soares, C., Santos, T.A. (Eds.), *Maritime Technology and Engineering 3*, vol. 1. Taylor & Francis Group, London, UK, pp. 409–418.

- Xu, H.T., Hinostroza, M.A., Guedes Soares, C., 2021. Modified vector field path-following control system for an underactuated autonomous surface ship model in the presence of static obstacles. *J. Mar. Sci. Eng.* 9 (6), 652.
- Xu, D.H., Huang, Y.J., Zhou, X.Q., Xu, H.T., 2023. Path following control for large inland ships in a restricted waterway using nonlinear terminal sliding mode method. *Ocean Eng.* 284, 115159.
- Xu, X.L., Pan, W., Huang, Y.B., Zhang, W.D., 2020. Dynamic collision avoidance algorithm for unmanned surface vehicles via layered artificial potential field with collision cone. *J. Navig.* 73 (6), 1306–1325.
- Xu, H.T., Rong, H., Guedes Soares, C., 2019. Use of AIS data for guidance and control of path-following autonomous vessels. *Ocean Eng.* 194, 106635.
- Yan, X., Jiang, D.P., Miao, R.L., Li, Y.L., 2021. Formation control and obstacle avoidance algorithm of a multi-USV system based on virtual structure and artificial potential field. *J. Mar. Sci. Eng.* 9 (2), 161.
- Yang, S.L., Huang, J., Xiang, X.B., Li, J.J., Liu, Y., 2023. Cooperative survey of seabed ROIs using multiple USVs with coverage path planning. *Ocean Eng.* 268, 113308.
- Ye, H., Li, W., Lin, S., Ge, Y., Lv, Q., 2024. A framework for fault detection method selection of oceanographic multi-layer winch fibre rope arrangement. *Measurement* 226, 114168.
- Yuan, S.Y., Li, Y., Bao, F.W., Xu, H.X., Yang, Y.P., Yan, Q.S., Zhong, S.Q., Yin, H.Y., Xu, J., Huang, Z.W., Lin, J., 2022. Marine environmental monitoring with unmanned vehicle platforms: present applications and future prospects. *Sci. Total Environ.* 858 (1), 159741.
- Zhang, W., Wang, K., Wang, S.A., Laporte, G., 2020. Clustered coverage orienteering problem of unmanned surface vehicles for water sampling. *Nav. Res. Logist.* 67 (5), 353–367.
- Zhu, X.H., Yan, B., Yue, Y., 2021. Path planning and collision avoidance in unknown environments for USVs based on an improved D* lite. *Appl. Sci.* 11 (17), 7863.
- Zhuang, J.Y., Zhang, L., Qin, Z.H., Sun, H.B., Wang, B.L., Cao, J.X., 2019. Motion control and collision avoidance algorithms for unmanned surface vehicle swarm in practical maritime environment. *Pol. Marit. Res.* 26, 107–116.